Journal of Physics G: Nuclear and Particle Physics

PAPER

Effect of the inelastic couplings on the scattering of alpha particles by ^{12}C at low energies

To cite this article: L C Chamon *et al* 2014 *J. Phys. G: Nucl. Part. Phys.* **41** 035101

View the article online for updates and enhancements.

You may also like

- Comparative role of the ^{7}Li(*n*,) reaction in Big Bang nucleosynthesis
N A Burkov, S B Dubovichenk, V Dzhazairov-Kakhramanov et al.
- The status and future of direct nuclear reaction measurements for stellar burning
M Aliotta, R Buompane, M Couder et al.
- Computational assessment of the cellular dosimetry and microdosimetry of the gadolinium electrons released during neutron capture therapy
Masud Golshani, Ali Asghar Mowlavi and Behnam Azadegan

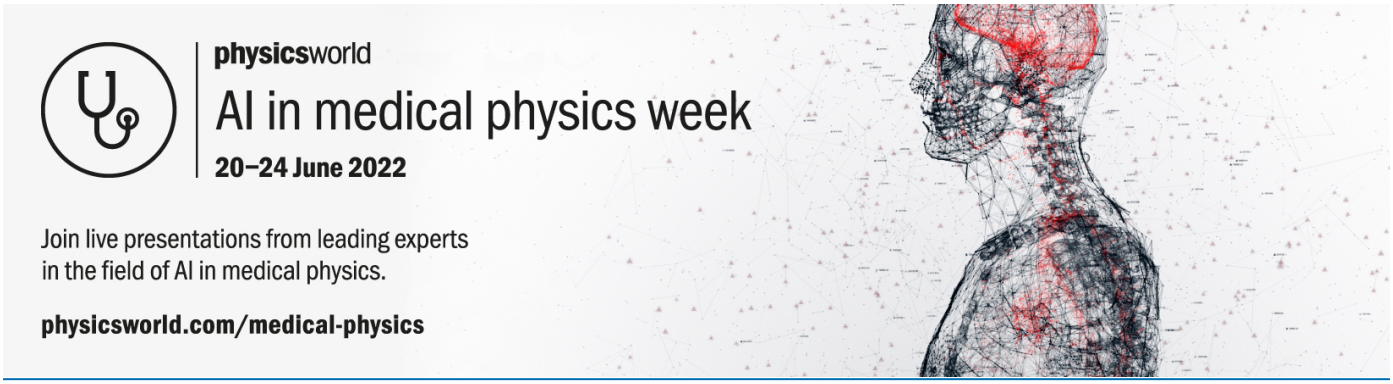

This content was downloaded from IP address 143.107.135.170 on 14/06/2022 at 16:45

IOP Publishing Journal of Physics G: Nuclear and Particle Physics

J. Phys. G: Nucl. Part. Phys. **41** (2014) 035101 (21pp) doi:10.1088/0954-3899/41/3/035101

Effect of the inelastic couplings on the scattering of alpha particles by ^{12}C at low energies

L C Chamon[1], L R Gasques[1], L F M Alves[1], V Guimarães[1], P Descouvemont[2], R J deBoer[3] and M Wiescher[3]

[1] Departamento de Física Nuclear, Instituto de Física da Universidade de São Paulo, Caixa Postal 66318, 05315-970, São Paulo, SP, Brazil
[2] Physique Nucléaire Théorique et Physique Mathématique, CP 229, Université Libre de Bruxelles (ULB), B 1050 Brussels, Belgium
[3] Department of Physics, University of Notre Dame, Notre Dame, IN 46556, USA

E-mail: lchamon@if.usp.br

Received 10 September 2013, revised 21 November 2013
Accepted for publication 6 January 2014
Published 5 February 2014

Abstract

We study the effects of the coupling to the first 2^+ ^{12}C excited state on the elastic scattering and capture reaction for the α + ^{12}C system. The flux absorption from the elastic channel to the capture reaction is simulated by a tiny imaginary part included in the optical potential. Our analyses show that the effect of the coupling is quite significant even at energies below the threshold of the inelastic channel. We also study the behavior of the polarization potential as a function of the energy and angular momentum.

Keywords: nuclear reactions, nuclear astrophysics, resonances

(Some figures may appear in colour only in the online journal)

1. Introduction

The collision between heavy-ions is a problem that involves a large number of degrees of freedom. Most often, this complicated problem is solved using a simplified approach. In the coupled-channel (CC) formalism (see e.g. [1]), usually a few reaction channels are explicitly taken into account in the numerical calculations, through the corresponding coupled equations, while the effect of the remaining channels is simulated by an effective optical potential. The contribution of these other channels, which should be included in the optical interaction, is named as polarization potential (PP). The PP is, in general, angular momentum and energy dependent, and also has a complicated shape that may include poles at some points. Even

 © 2014 IOP Publishing Ltd Printed in the UK

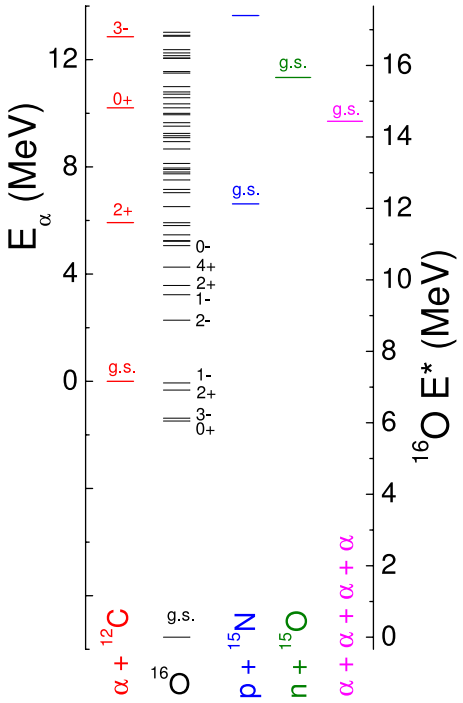

Figure 1. Energy levels of several channels involved in the α + ^{12}C scattering. The scale at the left side corresponds to the energy of the α particle at the laboratory frame of reference, while that at the right side represents the excitation energy in ^{16}O. The corresponding spin and parity are indicated for some levels.

so, in many elastic scattering data analyzes, quite simple models are assumed for the optical potential. Frequently, an angular momentum independent complex potential is assumed, where the real and imaginary parts have a Woods–Saxon shape with adjustable parameters. Another simplified model, often adopted in data analyzes, corresponds to the use of some folding model to calculate the bare nuclear interaction. In this approach, the real and imaginary parts of the optical potential are assumed to be proportional to the bare interaction. In this case, the normalization factors of the real and imaginary parts are usually considered adjustable parameters to fit the data. The behavior and properties of the optical potential have been extensively studied (see [2, 3]).

In earlier works [4, 5], we analyzed $\alpha + \alpha$ scattering at low energies. This is a particularly interesting system because there are no open reaction channels at low energies, except the $\alpha(\alpha,\gamma)^8$Be process which presents very small cross sections. Therefore, due to the lack of open reaction channels, the elastic scattering data analyzes for this system must be performed with an optical interaction without an imaginary part. We obtained a satisfactory description of the experimental elastic phase-shifts, for several angular momenta, with an energy and angular momentum independent real potential [5]. The same interaction also successfully describes the s-wave ground-state (g.s.) resonance of ^{8}Be.

The ^{12}C$(\alpha,\gamma)^{16}$O reaction is important for nucleosynthesis and stellar evolution, since it defines the ^{12}C/^{16}O ratio at the end of stellar core helium burning in massive stars. In figure 1, we present an energy level scheme of the main reaction channels involved in the α + ^{12}C scattering. The scale at the left side of the figure corresponds to the energy of the α particle at the laboratory frame of reference, while the scale on the right side represents the

excitation energy in ^{16}O. As seen in the figure, apart from the capture channel, ^{12}C(α,γ)^{16}O, the threshold for reactions occurs at $E_\alpha = 5.92$ MeV (see figure 1) and it corresponds to the inelastic excitation of the first ^{12}C 2^+ state ($E^* = 4.439$ MeV). The capture cross sections are very small and present resonances at energies that correspond to the low-lying levels in ^{16}O. These important characteristics make the α + ^{12}C reaction quite similar to that of the $\alpha + \alpha$ system mentioned above.

These considerations have motivated this study of α + ^{12}C scattering at low energies. Data for the corresponding capture channel have already been consistently analyzed within the *R*-matrix formalism, together with data of other related reactions such as ^{15}N(p,α)^{12}C and ^{12}C(α,α)^{12}C (elastic and inelastic channels, see e.g. [6]). In this work, the data analysis is performed in the context of the CC formalism, considering the coupling between the elastic and the first ^{12}C 2^+ inelastic channels. The (real) nuclear interaction for $\alpha + \alpha$ of [5] is adapted to the α + ^{12}C system, while the coupling between the elastic and inelastic channels is treated within the well-established vibrational model. The very small cross sections of the capture reaction are simulated in our CC calculations by including a tiny imaginary part in the optical potential. In this simple approach, experimental data for elastic phase-shifts, inelastic cross sections and capture reaction are reasonably described, although the *R*-matrix fits present better results. Indeed, the data fits are not our main purpose here. Since we have not included all the relevant channels in our CC calculations, the resulting cross sections are not intended to describe the data perfectly. The main goal of this work is to study the effects of the inelastic couplings on the elastic process. For the α + ^{12}C system, this is a quite interesting subject since, in this case, due to the lack of significant reaction cross sections, the imaginary part of the optical potential is expected to be almost negligible.

The paper is organized as follows. The next two sections present the data and the CC analyzes. The effects of the couplings and the behavior of the PP are discussed in section 4. In section 5, we show how the small imaginary potential is capable of simulating the capture reaction resonances. The main conclusions are found in section 6, while appendix presents details of the CC calculations.

2. The data set

Angular distributions for the α + ^{12}C* (2^+ $E^* = 4.439$ MeV) inelastic excitation have been measured at $7.85 \leqslant E_\alpha \leqslant 8.40$ MeV by Mitchel *et al* [7] and $8.30 \leqslant E_\alpha \leqslant 10.42$ by Ophel *et al* [8]. We obtained the corresponding total (integrated) inelastic cross sections from the first coefficient of the Legendre expansions which fit those distributions (see table 2 of [7] and figure 7 of [8]). However, those data were reported in arbitrary units. To normalize the lower energy data set of [7], we considered the *R*-matrix data fits of [9], and we used the normalized inelastic cross sections of [10] to normalize the data set of [8]. The results of the normalized experimental (total) inelastic cross sections are shown in figure 2 (blue circle and black star symbols). In [11], there are data, again in arbitrary units, for the γ-ray arising from the ^{12}C 2^+ de-excitation measured at $\theta = 45^\circ$. We have also normalized these data to match the corresponding cross sections with those from the other references. With this procedure, we could use the γ data set (small red circle symbols in figure 2) to represent the behavior of the total ^{12}C 2^+ inelastic cross section as a function of the energy of the α particle.

In figure 3, we present cross section data (from [12]) and *R*-matrix predictions (according to [9]) of different channels involved in the α + ^{12}C scattering: capture reaction, p + ^{15}N and ^{12}C 2^+ inelastic excitation. The positions of the energy levels for these three channels, as a function of the energy of the α particle, are represented at the top part of the figure. Obviously, the predictions for the p + ^{15}N and inelastic excitation cross sections vanish below

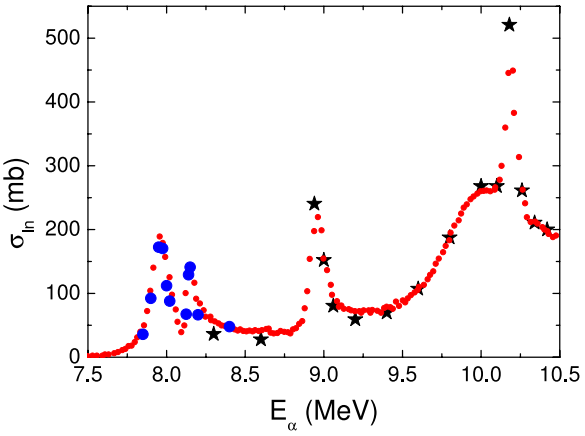

Figure 2. Integrated inelastic cross sections for the first ^{12}C 2^+ excited state as a function of the energy of the α particle. The blue circle and black star symbols are data obtained from [7] and [8], respectively. The small red circle symbols represent data of the corresponding γ-ray at $\theta = 45^\circ$ from [11]. All these data were normalized as described in the text.

the corresponding thresholds: the ground-state of $p + {}^{15}$N and the 2^+ state of $\alpha + {}^{12}$C (shown at the top of the figure). Clearly, the capture reaction presents cross sections which are several orders of magnitude smaller than those of the two other reaction channels. It is interesting to turn the attention to the fact that the cross sections for the three channels show resonances at energies that have a clear correspondence with some levels of the ^{16}O compound nucleus (see the dashed lines used as guide to the eyes in figure 3).

Figure 4 presents data for ^{12}C 2^+ inelastic excitation (red line) and ^{12}C$(\alpha, p)^{15}$N (blue circles). The (α, p) data set of this figure was actually obtained through cross sections of the inverse reaction, from [13–15], taking into account the principle of detailed balance. The black line in the figure represents total reaction cross sections obtained, through (A.13), from the modulus of the elastic S-matrix (which we have extracted from figure 10 of [16]) arising from elastic scattering data analyzes. For the energy region shown in figure 4, the inelastic and (α, p) are the only open reaction channels, with exception of the quite small cross sections related to the capture reaction and the four α break-up (for $E_\alpha \geqslant 9.7$ MeV). Thus, the total reaction cross section should be almost equal to the sum of the cross sections for these two channels. However, this is not the case for the total reaction cross section shown in figure 4, which is much larger than the sum in several energy regions. Part of this discrepancy can arise from our difficulty to obtain the values of the S-matrix from figure 10 of [16]. Another part is possibly related to slightly imprecise values for the modulus of the S-matrix obtained from the elastic scattering data analyzes in [16]. Again, the cross sections of figure 4 present resonances at energies related to levels of the compound nucleus. The resonance of the inelastic channel at about $E_\alpha = 10.2$ MeV is at a level that could correspond to two different states: ^{12}C 0^+ and ^{16}O 6^+. As discussed in the next paragraph, the experimental elastic phase-shifts indicate that this resonance in fact corresponds to the ^{16}O 6^+ state.

There is a large number of data for $\alpha + {}^{12}$C elastic scattering in the literature. We have considered the corresponding phase-shifts obtained from the data analyzes of [16–20]. In general, the sets of phase-shifts from different papers are consistent to each other and, then, we have compiled a less extensive set of values that is representative of the quite large amount of the available data. Figures 5–8 show the corresponding results (closed circles). The

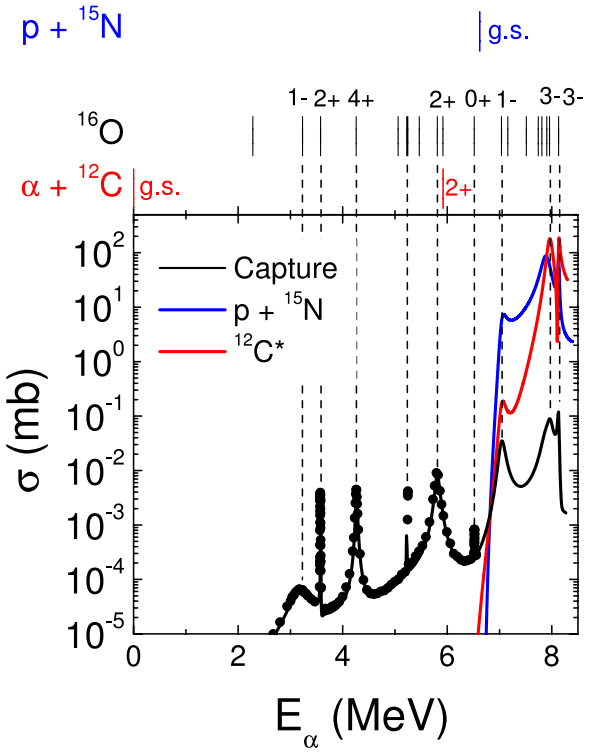

Figure 3. Cross sections for different channels involved in the scattering of the α particle on ^{12}C, as a function of the energy. The black circles and solid black line correspond to data (from [12]) and R-matrix calculations (according to [9]) for the capture reaction. The blue and red lines represent R-matrix calculations (also from [9]) for the $p + {}^{15}$N and $\alpha + {}^{12}$C* (2^{+}) reaction channels, respectively. In the top part of the figure, we present the energy levels of some channels. The dashed lines in the figure show the connection between the energy of some resonances with the levels of the compound nucleus.

phase-shift data also present resonances (in form of 'steps') at energies that correspond to the ^{16}O levels, as indicated by the black dashed lines in these figures. It is interesting to observe the consistency between the J (angular momentum) values of the phase-shifts with the spin and parity $(-1)^{J}$ of the corresponding ^{16}O levels. Also the 'width of the steps' are consistent with the level widths. In particular, the $J = 6$ phase-shift data of figure 8 show a resonance at $E_{\alpha} \approx 10.2$ MeV, indicating that the resonance in the inelastic cross section at this same energy (see figure 4) is, in fact, related to the 6^{+} state of the ^{16}O.

3. The CC data analyzes

Besides the elastic, the only channel explicitly coupled in our calculations corresponds to the first excited state of ^{12}C. We tried to fit the data set for $\alpha + {}^{12}$C within the framework of the vibrational and rotational models, and also with a hybrid model that would represent a rotation–vibration approach. The best results were obtained with the vibrational model. Probably, the first ^{12}C 2^{+} state cannot be completely described within collective models like the vibrational or rotational. Even so, as we have free parameters to fit the data, we assumed the vibrational model to perform our final calculations.

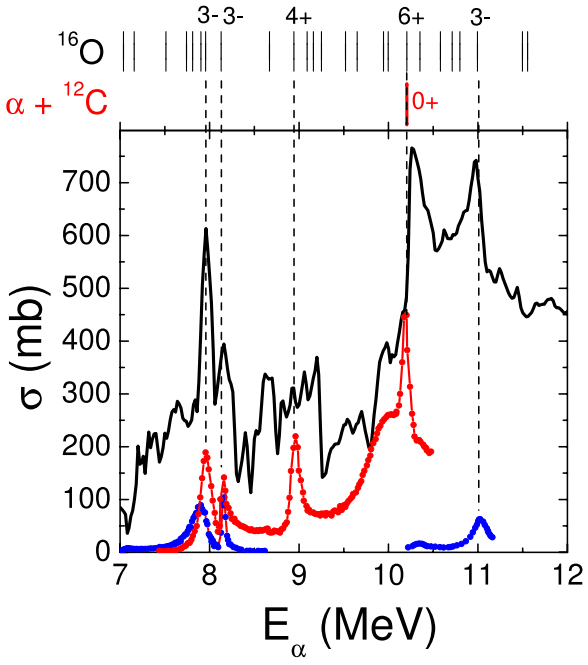

Figure 4. Cross section data for the ^{12}C 2^+ inelastic excitation (red line) and for the $p+$ ^{15}N channel (from [13–15]—blue circles). The black line represents total reaction cross sections obtained through the modulus of the elastic S-matrix extracted from [16]. The meaning of the top part of the figure and of the dashed lines is the same as in figure 3.

Appendix presents a detailed description of the approach that we assumed in our CC calculations. Basically, we have solved numerically the following set of coupled equations:

$$\left\{\frac{-\hbar^2}{2\mu}\left[\frac{\mathrm{d}^2}{\mathrm{d}R^2}-\frac{J(J+1)}{R^2}\right]+V_N(R)+V_C(R)+\mathrm{i}W(R)-E\right\}F_{0J}(R) = -\sum_{\ell} V_{J\ell}(R)F^{(J)}_{2\ell}(R), \tag{1}$$

$$\left\{\frac{-\hbar^2}{2\mu}\left[\frac{\mathrm{d}^2}{\mathrm{d}R^2}-\frac{\ell(\ell+1)}{R^2}\right]+V_N(R)+V_C(R)+\mathrm{i}W(R)-(E-E^*)\right\}F^{(J)}_{2\ell}(R) = -V_{J\ell}(R)F_{0J}(R), \tag{2}$$

with $\ell = J-2, J, J+2$ ($\ell \geqslant 0$), resulting in four coupled equations for each total angular momentum J. The terms at the right side of (1) represent the couplings of the inelastic $F^{(J)}_{2\ell}$ to the elastic F_{0J} wave-functions. In these equations, the coupling potentials are given by

$$V_{J\ell} = \mathrm{i}^{J-\ell}\frac{C^{J\,2\,\ell}_{000}}{\sqrt{4\pi}}\left[\beta_C R_0^2\frac{3Z_1Z_2e^2}{5}f(R)-\beta_N R_0\frac{\mathrm{d}V_N}{\mathrm{d}R}\right], \tag{3}$$

$$C^{J\,2\,J}_{000} = -\sqrt{\frac{J(J+1)}{(2J-1)(2J+3)}}, \tag{4}$$

$$C^{J\,2\,J-2}_{000} = \sqrt{\frac{3J(J-1)}{2(2J-1)(2J+1)}}, \tag{5}$$

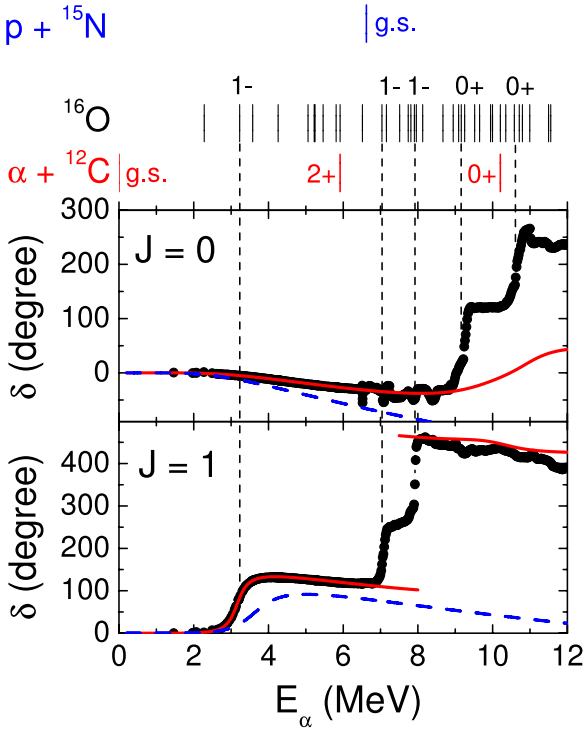

Figure 5. Experimental elastic phase-shifts for $J = 0$ and 1. The solid red and dashed blue lines represent the results of our calculations, with or without the coupling to the ^{12}C 2^+ state, respectively. The meaning of the top part of the figure and of the dashed (black) lines is the same as in figure 3.

$$C^{J\,2J+2}_{000} = \sqrt{\frac{3(J+1)(J+2)}{2(2J+1)(2J+3)}}, \tag{6}$$

where R_0 is the undeformed radius of ^{12}C, and β_C and β_N are the Coulomb and nuclear deformation parameters, respectively.

The boundary conditions for the elastic and inelastic wave-functions are represented, respectively, by

$$F_{0J}(R \to \infty) = \frac{\mathrm{i}}{2}[H^-_J(R) - S_{0J}H^+_J(R)], \tag{7}$$

$$F^{(J)}_{2\ell}(R \to \infty) = -\frac{\mathrm{i}}{2}S_{2\ell}H^+_\ell(R), \tag{8}$$

$$H^\pm_\ell = G_{C\ell} \pm \mathrm{i}F_{C\ell}, \tag{9}$$

where $G_{C\ell}$ and $F_{C\ell}$ are the Coulomb wave-functions and S_{0J} and $S_{2\ell}$ are the elastic and inelastic S-matrices. The elastic S-matrix can be written in terms of the corresponding phase-shifts, δ_J, as:

$$S_{0J} = |S_{0J}|\mathrm{e}^{2\mathrm{i}\delta_J}. \tag{10}$$

For energies below the threshold of the inelastic channel, the inelastic S-matrix vanishes since (8) cannot be satisfied. In this case, the inelastic wave-function is proportional to the Whittaker function [21].

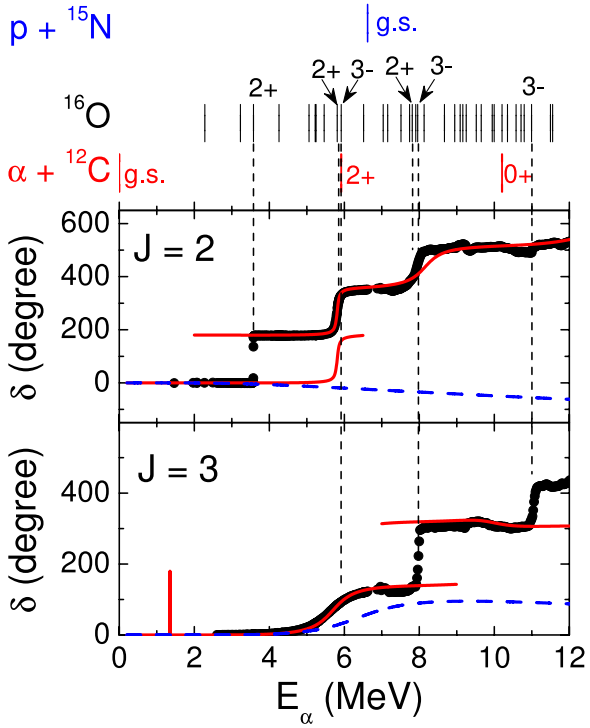

Figure 6. The same as figure 5, but for $J = 2$ and 3.

The nuclear interaction is given by

$$V_N(R) + \mathrm{i}W(R) = (N_R + \mathrm{i}N_I)V_0(R), \tag{11}$$

where $V_0(R)$ is the nuclear interaction proposed for the $\alpha + \alpha$ system [5] adapted to the present case. N_I is the normalization factor for the imaginary part of the interaction, which simulates the absorption of flux from the elastic and inelastic channels to the capture reaction. As the corresponding cross sections are very small, we obtained N_I values of the order of 10^{-9}.

The nuclear deformation, β_N, and the normalization factor for the real part of the interaction, N_R, were considered as adjustable parameters to fit the data. Furthermore, we also assumed that N_R could have different values for different total angular momenta J. We consider that $V_0(R)$ is a realistic model for the nuclear potential and, therefore, the N_R parameter value was assumed to vary only in the region $0.8 \leqslant N_R \leqslant 1.2$. Also the β_N value was limited to the region $\beta_N \leqslant 0.6$. In these conditions, the β_N and N_R values were obtained from the fit of the elastic phase-shifts at the region of lower energies. According to (10), the phase-shifts can be modified by $n \times 180^\circ$, n integer, without affecting the elastic S-matrix. Thus, in some energy regions, the theoretical phase-shifts (red lines in figures 5–8) were displaced by $n \times 180^\circ$. Our theoretical results miss some resonances, but the overall agreement between the theoretical and experimental phase-shifts is good, mainly at the region of lower energies (see figures 5–8). Due to the restrictions imposed on the values of the adjustable parameters, in this low energy region ($E_\alpha \leqslant 7$ MeV) two resonances could not be described: 2^+ at about 3.6 MeV and 4^+ at about 5.2 MeV. It is possible to obtain resonances at these energies within our theoretical approach, but with width values much larger than those observed in the data and, in this case, the adjustments of resonances at other energies become worse.

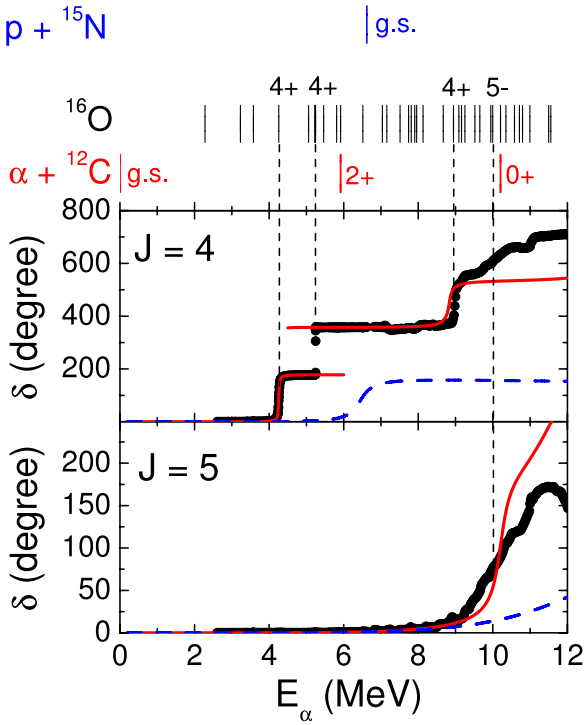

Figure 7. The same as figure 5, but for $J = 4$ and 5.

As earlier mentioned, the first 2^+ excited state of ^{12}C was the only reaction channel included in the CC calculations. Accordingly, we do not expect to describe the experimental data set with a high degree of precision. Taking this into account, the general trend of the experimental inelastic cross section is reasonably reproduced by our theoretical calculations, as shown in figure 9.

In our calculations, the capture cross section is associated with the absorption arising from the imaginary part of the potential: $\sigma_{\rm C} = \sum \sigma_{CJ}$, where [22]

$$\sigma_{CJ} = -(2J+1)\frac{4\pi}{kE}\int_0^\infty W(R)\,|F(R)|^2\,{\rm d}R, \quad \text{with} \quad |F(R)|^2 = |F_{0J}|^2 + \sum_\ell \left|F_{2\ell}^{(J)}\right|^2. \qquad (12)$$

Figure 10 contains data [12] and CC results for the astrophysical S factor of the capture reaction. The S factor is related to the total cross section by $S = E\,{\rm e}^{2\pi\eta}\sigma_c$, where η is the Sommerfeld parameter. The N_I parameter values for $J = 1$, 2, 3 and 4 were adjusted to fit the data. The corresponding results of the CC partial cross sections are also shown in figure 10. As can be seen in this figure, our theoretical results (solid black line) describe the capture data quite well. The position and width of the capture reaction resonances are intrinsically related to the behavior of the respective elastic phase-shifts as a function of the energy. Therefore, the centroid and width of the capture reaction resonances are naturally reproduced in our calculations, due to our fits of the elastic phase-shifts. The N_I parameter is then responsible just to provide the right magnitude of the capture reaction cross section. However, our theoretical calculations predict an extremely narrow resonance for $J = 3$ at $E_\alpha \approx 1.3$ MeV, which corresponds to an excitation energy of about 8.2 MeV in ^{16}O (with minuscule 2 eV of width). In fact, also the theoretical phase-shifts for $J = 3$ present a very narrow 180° jump at $E_\alpha \approx 1.3$ MeV (see figure 6). There is a known 3^- level in ^{16}O at the excitation energy of 6.13 MeV, but no level has been experimentally

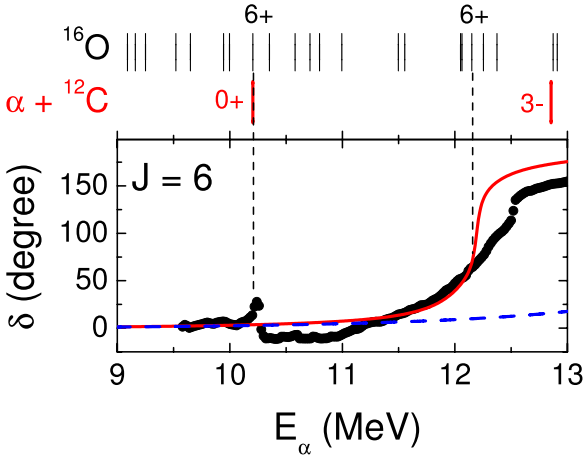

Figure 8. The same as figure 5, but for $J = 6$.

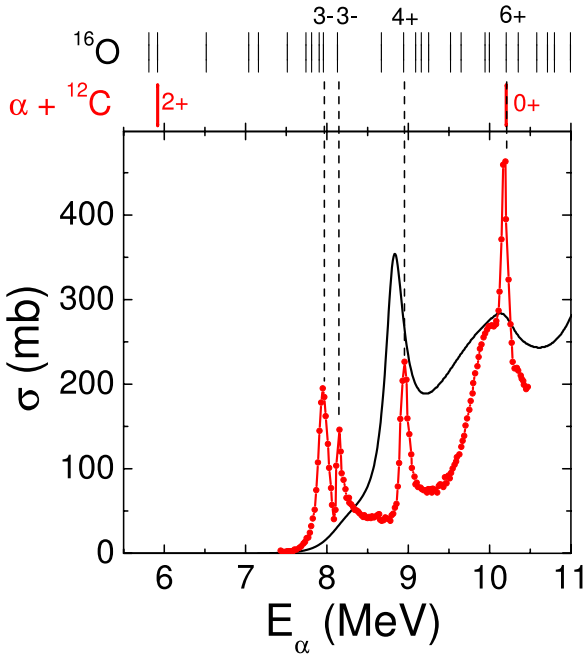

Figure 9. Data (red line) and theoretical results (black line) for the integrated ^{12}C 2^+ inelastic cross section.

observed at $E^* = 8.2$ MeV. It simply might be a spurious result of our calculations. On the other hand, there is an alternative explanation for these facts. Considering its quantum numbers, the 3^- ^{16}O state could be an one-particle-one-hole excitation, or it could also be a molecular excitation, or even a mixture of both. Within the hypothetical case of a mixture, both with $E^* \approx 8$ MeV, due to mixing of them (or with more molecular states) the lower eigenstate is pushed below the barrier to about 6 MeV and the other moves up to 11.5 MeV in the spectrum of ^{16}O. Therefore, the 3^- state at $E^* = 8.2$ MeV obtained in the present model is conceivable even if there is no observed state in the ^{16}O spectrum at this energy.

Table 1. Values of N_R and N_I for the indicated angular momentum J obtained from our CC analyzes. The readjusted values of the normalization factors, N_{RA}, used to simulate the CC results for phase-shifts from calculations without couplings are also presented.

J	N_R	N_I	N_{RA}	N_{RA}/N_R
0	0.8950	0	0.986	1.10
1	0.9688	0.38×10^{-9}	0.998	1.03
2	0.9167	0.81×10^{-8}	1.150	1.25
3	0.9750	1.22×10^{-9}	1.012	1.04
4	0.8952	0.52×10^{-9}	0.945	1.06
5	0.9650	0	1.055	1.09
6	0.8674	0	0.934	1.08

Since, in principle, N_I might have some energy dependence, there is no guarantee that the present theoretical calculations can be reliably extrapolated to the very low energy region that would be interesting for astrophysics. Indeed, the results of the R-matrix calculations presented in figure 1 of [6] are quite similar to our CC results for $J = 1$ at $E_\alpha \approx 3$ MeV, but these two calculations provide quite different behaviors for the $E1$ contribution in the region of low energies. Even so, we provide the present total S factor value for the capture reaction at the relevant Gamow energy of $E_\alpha = 0.3$ MeV: $S = 95$ keV b. This result is about 40% smaller than the values obtained from R-matrix calculations, which are typically around 160 keV b (e.g. [6]).

The best value for the deformation parameter obtained from our fits is $\beta_N = 0.285$. The N_R and N_I values resulting from our analyzes are presented in table 1. As already mentioned, the order of magnitude of the N_I values is 10^{-9}. The N_R values (for the different J) spread by less than 6% around $N_R \approx 0.92$ (which in turn is quite close to the unity). This small variation may arise from the polarization effects due to other reaction channels not included in our CC calculations. Indeed, as we will see in the next section, the effects of the PP due to the inelastic 2^+ coupling do represent a renormalization of about 10% in comparison with the bare interaction.

4. The effects of the inelastic coupling

A first insight about the effects of the ^{12}C 2^+ inelastic coupling on the elastic scattering process can be provided just by turning the coupling off ($\beta_N = \beta_C = 0$) and recalculating the phase-shifts. The corresponding results are presented as dashed blue lines in figures 5–8. The effect is quite significant for all J values, and particularly strong for $J = 2$ where two resonances observed in the CC results are washed out when the coupling is turned off.

As an attempt of obtaining a 'quantitative measurement' of the effects of the coupling, we performed other calculations with $\beta_N = \beta_C = 0$, but this time renormalizing the N_R values in order to match the corresponding phase-shifts with those obtained within the context of the CC calculations. The corresponding phase-shift results are shown in figure 11 as dotted black lines. For comparison, the CC phase-shifts and also those obtained just turning the coupling off (without renormalizing N_R) are shown in figure 11, as solid red and dashed blue lines, respectively. With this procedure, some resonances observed in the CC case for $J = 0$ and 4 are missed within the readjusted case. Particularly for $J = 2$, we could not obtain any readjusted N_R value to reproduce, with reasonable degree of similarity, the CC phase-shifts at low energies (see figure 11). Table 1 provides the values of the readjusted normalization factors (N_{RA}) and their corresponding ratios to the CC N_R values. The N_{RA} values are roughly

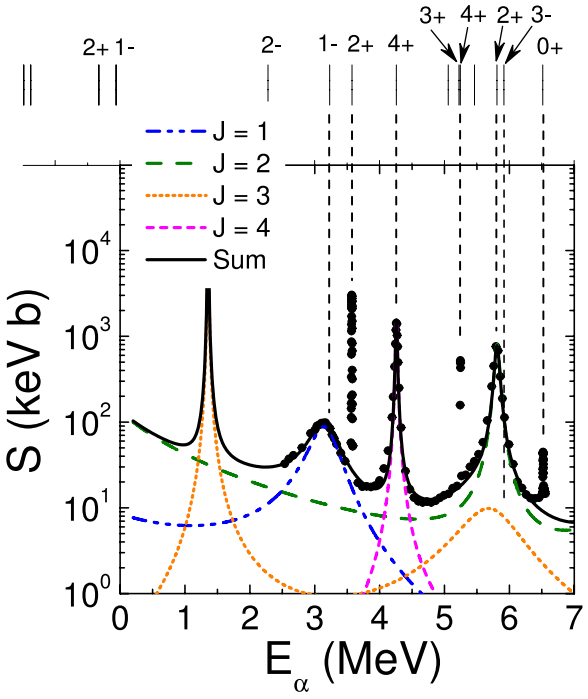

Figure 10. Experimental (closed circles) and theoretical CC (solid black line) astrophysical S factors for the capture reaction. The CC partial contributions of some angular momenta are also represented in the figure. The top part of the figure presents levels of the ^{16}O compound nucleus, including some in the sub-threshold energy region for $\alpha + {}^{12}$C.

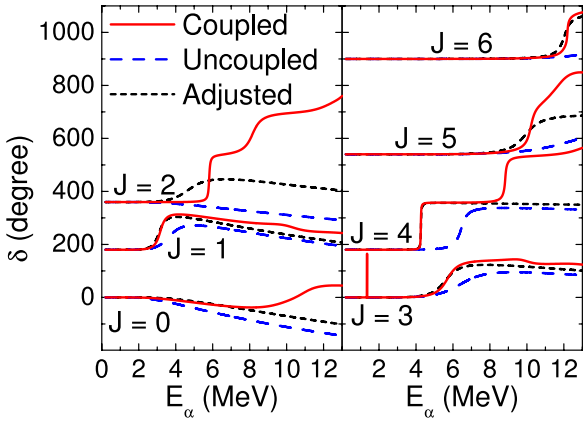

Figure 11. Theoretical phase-shifts obtained with (solid red lines) and without (dashed blue lines) coupling. The dotted black lines in the figure correspond to calculations without coupling, but with different N_R values which were adjusted to approach the CC results at low energies.

10% larger than the N_R ones (from 3% for $J = 1$ to 25% for $J = 2$). In this limited sense, as stated in the last section, the effect of the polarization due to the inelastic coupling represents a renormalization of the bare interaction by about 10%.

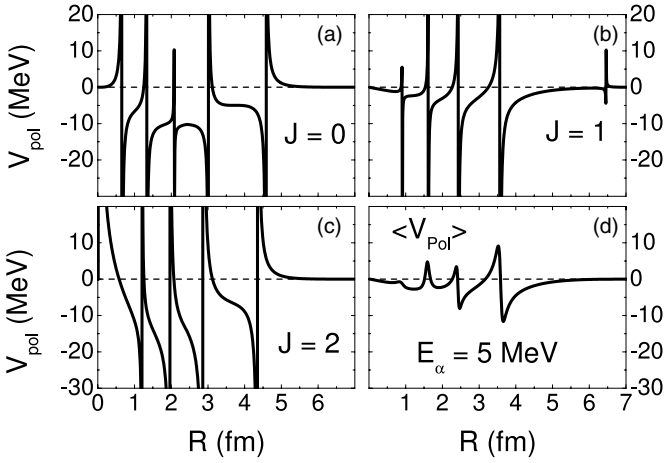

Figure 12. Real part of the local-equivalent polarization potential at $E_\alpha = 5$ MeV for $J =$ (a) 0, (b) 1 and (c) 2. In (d), we show the mean, angular momentum independent, polarization potential obtained from (16).

Due to the small number of open reaction channels at low energies, the study of the behavior of the PP is particularly interesting in the present case of $\alpha + {}^{12}$C. The local equivalent PP corresponding to the inelastic channel is defined as

$$U_{\rm pol} = -\frac{1}{F_{0J}(R)} \sum_{\ell} V_{J\ell}(R) F_{2\ell}^{(J)}(R). \tag{13}$$

We name the real and imaginary parts of $U_{\rm pol}$ as $V_{\rm pol}$ and $W_{\rm pol}$, respectively. With this, (1) can be re-written as

$$\left[\frac{-\hbar^2}{2\mu}\left[\frac{{\rm d}^2}{{\rm d}R^2} - \frac{J(J+1)}{R^2}\right] + U_{\rm Op}(R) + V_C(R)\right] F_{0J}(R) = E F_{0J}(R), \tag{14}$$

where

$$U_{\rm Op}(R) = V_N(R) + V_{\rm pol}(R) + {\rm i}[W(R) + W_{\rm pol}(R)]. \tag{15}$$

Clearly, (14) is the usual Schrödinger equation for one single channel (elastic) with an optical potential given by (15).

Taking into account (13), the PP is energy and angular momentum dependent. Figures 12(a)–(c) show the real part of the polarization for $J = 0$, 1 and 2, respectively, at $E_\alpha = 5$ MeV. This energy is below the threshold and, therefore, the imaginary part of the polarization vanishes. Due to the presence of the elastic wave-function in the denominator of (13), the local equivalent PP has poles where this wave-function vanishes. On the other hand, the probability of finding the system around these particular distances also vanishes since it is proportional to the square of the wave-function. In this sense, the corresponding poles in the polarization are not significant. In order to avoid this complication, we define a mean (average over the angular momenta) PP as

$$\langle U_{\rm pol}(R)\rangle = \langle V_{\rm pol}(R)\rangle + {\rm i}\langle W_{\rm pol}(R)\rangle = \frac{\sum_J a_J |F_{0J}(R)|^2 U_{\rm pol}(R)}{\sum_J a_J |F_{0J}(R)|^2}, \tag{16}$$

where

$$a_J = (2J+1)|1 - S_{0J}|^2. \tag{17}$$

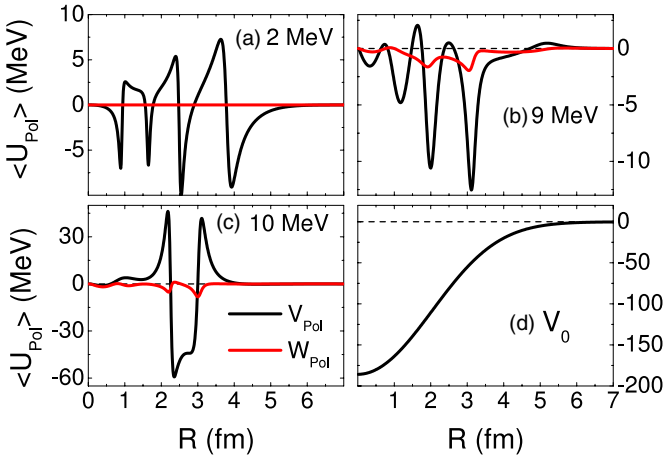

Figure 13. Real (black lines) and imaginary (red lines) parts of the mean polarization potential for E_α = (a) 2, (b) 9 and (c) 10 MeV. For comparison, in (d) we show the nuclear bare interaction.

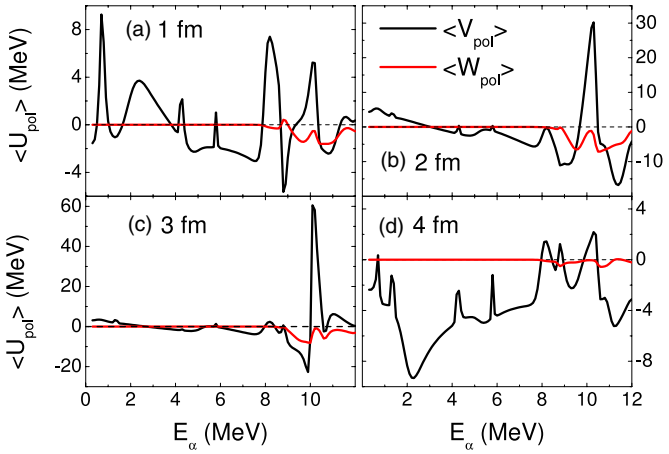

Figure 14. Real (black lines) and imaginary (red lines) parts of the mean polarization potential, as a function of the bombarding energy, for different distances of the interaction: R = 1, 2, 3 and 4 fm. At these radii, the strengths of the bare nuclear interaction (V_0) are, respectively, −163.8, −110.5, −55.1 and −19.8 MeV.

This expression is quite similar to that proposed in [23], except for the definition of the a_J coefficients, assumed in that paper as $a_J = (2J + 1)(1 - |S_{0J}|^2)$. Expression (17) is more appropriated in the present case because below the reaction threshold all the elastic S-matrix elements have unitary modulus. In figure 12(d), we can notice that the poles actually disappear in the case of the mean PP at $E_\alpha = 5$ MeV.

Figures 13(a)–(c) show the real (black lines) and imaginary (red lines) parts of the mean PP, as a function of the distance, for three different energies. For comparison, in figure 13(d) we also present the nuclear bare interaction V_0. The behavior of the mean PP as a function of the energy is shown in figure 14 for four different distances of interaction. As can be seen in figures 13 and 14, the shape and also the energy dependence of the polarization present

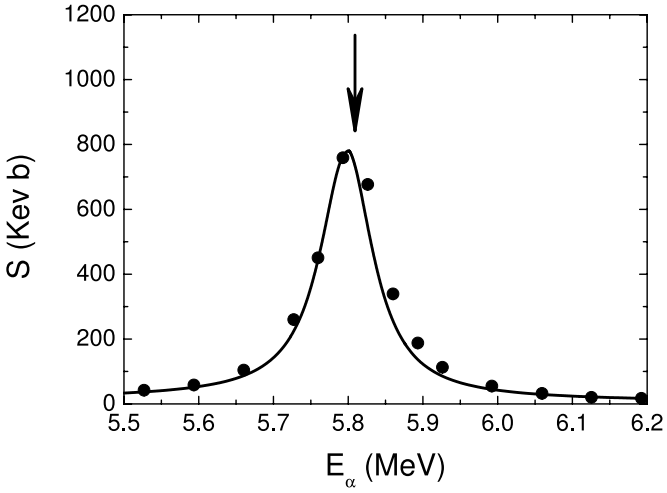

Figure 15. Experimental and theoretical CC astrophysical S factors, for the capture reaction, in an energy region around the 2^+ resonance. The 2^+ ^{16}O level positioned at $E_\alpha \approx 5.81$ MeV is indicated by the arrow in the figure. This same resonance is also shown in figure 10 in another scale.

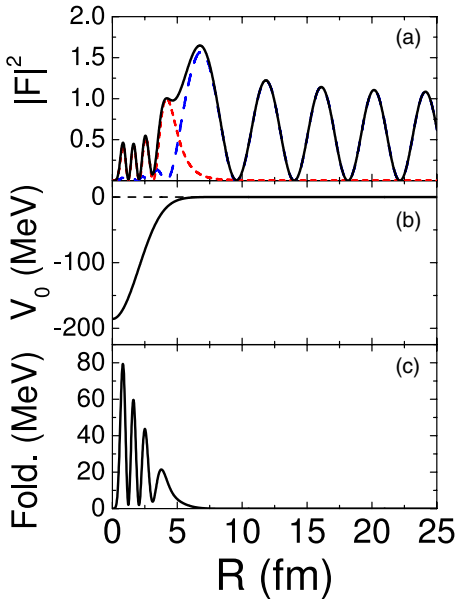

Figure 16. (a) Square of the elastic ($|F_{0J}|^2$, dashed blue line), inelastic ($\sum_\ell |F_{2\ell}^{(J)}|^2$, short-dashed red line) and total ($|F(R)|^2 = |F_{0J}|^2 + \sum_\ell |F_{2\ell}^{(J)}|^2$, solid black line) wave-functions, for $J = 2$ at $E_\alpha = 7$ MeV, as functions of the radius. (b) The bare nuclear interaction $V_0(R)$. (c) The folding between the potential and the square of the total wave function: Fold. $= -V_0(R) \times |F(R)|^2$.

quite complex structures. It is thus remarkable that just a small renormalization of the bare interaction can partially simulate the effects of the PP on the elastic phase-shifts (as illustrated in figure 11).

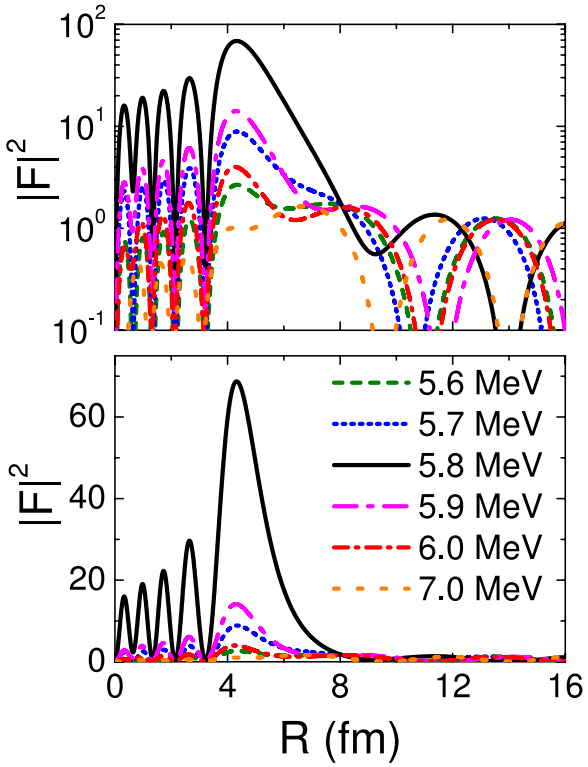

Figure 17. Square of total wave-functions for $J = 2$ at different energies, as indicated in the figure. Note that the change from linear (bottom) to logarithmic (top) scale.

5. The simulation of the capture reaction

As already mentioned, we have used a tiny imaginary potential, which is proportional to the nuclear bare interaction, $W(R) = N_I V_0(R)$, to simulate the absorption of flux from the elastic and inelastic channels to the capture process. The corresponding cross section was obtained through (12). In this section, we discuss the reason for the success of this procedure in some cases.

We take as example the 2^+ excited state of the ^{16}O, corresponding to the excitation energy of 11.52 MeV with width of 0.071 MeV. In the laboratory frame of reference, this resonance is positioned at $E_\alpha = 5.81$ MeV with width of 0.095 MeV. The data and the results of the CC calculations for the respective capture S factor are presented in figure 15. As can be seen in this figure, our theoretical results are in quite good agreement with the data. To understand the reason for that, we should study the behavior of the wave-function for $J = 2$ at energies around 5.81 MeV, as follows.

Figure 16(a) shows the square of the elastic, inelastic and total wave-functions, for $J = 2$ at $E_\alpha = 7$ MeV, as a function of the radius. In figure 16(b), we present the nuclear bare interaction, and, in figure 16(c), one can see the folding of the interaction with the square of the total wave-function: $-V_0(R) \times |F(R)|^2$. Considering that $W(R)$ is proportional to $V_0(R)$, this folding basically represents the integrand of expression (12), which is used to calculate the capture cross section. As $V_0(R)$ has a short range, the folding values become significant only for small distances (compare figure 16(a) with (c)). That is the key idea of using the

imaginary potential proportional to the nuclear interaction (with the purpose of simulating the absorption from the capture reaction). If the system has large values for the wave-function at small R values, which means a large probability of finding the α particle quite close to the ^{12}C, then the capture reaction cross section should also be large. This seems to be a reasonable idea which is automatically contained in the folding of (12) according to the model proposed here. Indeed, the description of the fusion process through an inner imaginary potential is an idea already applied in many works. Here, we have just adapted this procedure to the resonant process of the capture reaction.

Figure 17 presents the square of the total $J = 2$ wave-function at several energies around the 2^+ resonance. Let us focus on the region of small R values of this figure. The wave-function is relatively small at $E_\alpha = 5.6$ MeV (about two widths far from the centroid of the resonance). The wave-function values become larger for increasing energies, reaching maximum values at about $E_\alpha = 5.8$ MeV (centroid of the resonance). Then the wave-function values become smaller for higher energies. This resonant behavior of the wave-function results, thus, through (12), in the respective behavior of the S factor shown in figure 15.

Our model works well because the capture cross sections are very small and, consequently, N_I has tiny values. This results in quite small strength for the imaginary potential, which is an important condition to guarantee that the imaginary potential does not affect the wave-function. In fact, we checked that the wave-functions and also the elastic phase-shifts present totally negligible changes if we turn the imaginary potential off (using $N_I = 0$). Thus, the resonances in the cross sections are contained, in some form, in the real part of the interaction, since it is responsible for the resonant behavior of the wave-function.

6. Summary and conclusion

We have chosen the α + ^{12}C system to study the effects of the inelastic couplings on the elastic scattering and capture reaction processes. This choice was made due to several reasons. First because this system presents a small number of open reaction channels at low energies, which allowed us to assume an almost negligible (except by the tiny N_I) imaginary potential in our analyzes. Furthermore, the adopted vibrational model for the inelastic coupling is well established. In addition, there is a large set of data available for this system. The data fit was not the main purpose of this work. Even so, we obtained a reasonable description of experimental elastic phase-shifts, inelastic cross sections and S factor for capture reactions, although the precision of our results is not comparable with the remarkable data fits obtained with R-matrix calculations (see e.g. [6, 24]).

As we have demonstrated, the effects of the coupling on the elastic phase-shifts are significant even at energies well below the threshold. The shape, angular momentum and energy dependencies of the corresponding PP are quite complicated. Despite its complexity, the effects of the PP (inelastic coupling) on the elastic phase-shifts can be simulated, only partially, with a J-dependent renormalization of the bare interaction of roughly 10%.

Our model includes a simulation for the absorption of the flux by the capture reaction. With this model, we described some resonances observed in the capture cross sections, which are closely related to the behavior of the corresponding elastic phase-shifts as a function of the energy. Somehow these resonances are contained in the real part of the nuclear interaction between the α and the ^{12}C nuclei, which ultimately is the responsible for the resonant behavior of the wave-function. Our analyzes clearly show that a few of these resonances are related to the inelastic coupling since they are washed out when it is turned off. On the other hand, there are also other resonances observed in the data set that could not be described by our calculations.

A logical next step of this work would be to increase the number of channels explicitly included in the CC calculations. The present approach could be easily adapted to include the 4^+ state of ^{12}C, which probably has significant effects on the elastic phase-shifts and capture reaction. Other natural candidates would be the (α, p) and (α, γ) channels which, however, are not simple direct channels since the compound nucleus certainly plays an important role in these processes. Thus, possibly a new model for the coupling of this kind of channels is required to appropriately describe such processes.

Acknowledgments

We thank Dr Daniel Schürmann for providing us with the data of [12, 17] in the form of tables. This work was partially supported by the Fundação de Amparo à Pesquisa do Estado de São Paulo (FAPESP), the Conselho Nacional de Desenvolvimento Científico e Tecnológico (CNPq), and the Astrophysics Group of the Instituto de Estudos Avançados da Universidade de São Paulo.

Appendix. The coupled-channel calculations

A general description of CC calculations for heavy-ion systems can be found, for instance, in [1]. In this section, we present the approach assumed in our CC calculations within the context of the vibrational model, which is similar to that reported in [25]. In the present case, the α + ^{12}C (g.s.) is the entrance channel, while α + ^{12}C (g.s.) and ^{12}C (2^+ $E^* = 4.439$ MeV) are the possible exit channels.

The radius of the deformed ^{12}C nucleus is described by a quadrupole deformation written, in its intrinsic frame of reference, as

$$R(\theta_I, \phi_I) = R_0 \left[1 + \sum_m a_{2m} Y_{2m}(\theta_I, \phi_I) \right], \tag{A.1}$$

with

$$\begin{aligned} a_{20} &= \beta \cos\gamma \\ a_{21} &= a_{2-1} = 0 \\ a_{22} &= a_{2-2} = \beta \sin\gamma / \sqrt{2}. \end{aligned} \tag{A.2}$$

In the laboratory frame of reference, where the z-axis has the same direction of the beam, the target radius is given by

$$R(\theta_L, \phi_L) = R_0 \left[1 + \sum_m \alpha^*_{2m} Y_{2m}(\theta_L, \phi_L) \right], \tag{A.3}$$

with

$$\alpha_{2m} = \sum_{m'} a_{2m'} D^{2*}_{mm'}(\theta_1, \theta_2, \theta_3), \tag{A.4}$$

where $D^{2*}_{mm'}$ is the rotation matrix and $\theta_i \equiv (\theta_1, \theta_2, \theta_3)$ is the set of the Euler angles between both frames of reference (see e.g. [26]).

As usual (see e.g. [25, 27–29]), the deformed nuclear and Coulomb interactions are expanded to first order in the corresponding deformation parameters as

$$U(\vec{R}, \alpha) = V_N(R) + V_C(R) + \mathrm{i}W(R) - \left[\frac{\mathrm{d}V_N}{\mathrm{d}R} - R_0 \frac{3Z_1 Z_2 e^2}{5} f(R) \right] R_0 \sum_m \alpha^*_{2m} Y_{2m}(\theta, \phi), \tag{A.5}$$

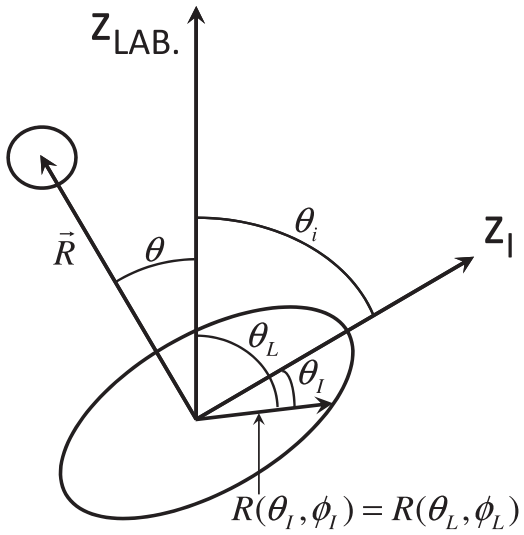

Figure A1. Schematic representation of the collision between a spherical (α) and a deformed (^{12}C) nucleus. Z_I and $Z_{\mathrm{LAB.}}$ are Z axes in the intrinsic and laboratory frames of reference, respectively. θ_i represents the set of Euler angles between these frames. The radius of the deformed nucleus at a particular direction is shown in the figure and can be described through (A.1) or (A.3) in both systems of references. Finally, the figure also shows the $\vec{R}$ vector that connects the centers of mass of the two nuclei.

where $f(R) = 1/R^3$ for $R \geqslant R_0$ and $f(R) = R^2/R_0^5$ for $R \leqslant R_0$, $R_0 = 1.06\, A_2^{1/3}$ fm, A_1, A_2, Z_1, Z_2 are the numbers of nucleons and protons of the alpha and ^{12}C nuclei. In (A.5), R is the distance between the centers of mass of both nuclei and (θ, ϕ) represents the direction of $\vec{R}$ in the laboratory frame of reference. Figure A1 shows a schematic representation of the collision.

In (A.5), $V_N(R)$ and $V_C(R)$ are the central parts of the nuclear and Coulomb potentials, respectively, and $W(R)$ is a quite small imaginary potential used to simulate the absorption from the capture reaction. We assume $V_N(R) = N_R\, V_0(R)$ and $W(R) = N_I\, V_0(R)$, where N_R and N_I are normalization factors for the real and imaginary parts of the optical potential, and $V_0(R)$ is the nuclear interaction proposed in [5]:

$$V_0(R) = \int \rho_1(r_1)\rho_2(r_2)v(\vec{R} - \vec{r_1} + \vec{r_2})\,\mathrm{d}\vec{r_1}\,\mathrm{d}\vec{r_2}, \tag{A.6}$$

with

$$v(\vec{r}) = -U_0 \mathrm{e}^{-(r/a)^2}, \tag{A.7}$$

$U_0 = 87.226$ MeV and $a = 0.95$ fm. In (A.6), $\rho_i(r_i)$ represent the undeformed matter densities of the nuclei, which we associate with the corresponding charge densities multiplied by two (due to the normalization). In our analyzes, N_R is close to the unity and N_I is of the order of 10^{-9}. Also the Coulomb potential has been obtained from folding procedures:

$$V_C(R) = \int \rho_{C1}(r_1)\rho_{C2}(r_2)\frac{e^2}{|\vec{R} - \vec{r_1} + \vec{r_2}|}\,\mathrm{d}\vec{r_1}\,\mathrm{d}\vec{r_2}. \tag{A.8}$$

The undeformed ground-state charge distributions, $\rho_{Ci}(r_i)$, were obtained from [30].

The Schrödinger equation for the present case is

$$[\hat{T} + \hat{H}(\alpha) + U(\vec{R}, \alpha)]\Psi(\vec{R}, \alpha) = E\Psi(\vec{R}, \alpha), \tag{A.9}$$

where α represents the complete set of deformation coordinates: β, γ, θ_i. In (A.9), $\hat{T}$ is the kinetic energy operator, $\hat{H}$ is the intrinsic Hamiltonian (vibrational model) of the deformed nucleus (^{12}C) and Ψ is the total wave-function of the system. We expand the wave-function into a sum involving the total angular momentum (J) as

$$\Psi = \sum_J \frac{1}{kR}\sqrt{4\pi\,(2J+1)}\;\mathrm{e}^{\mathrm{i}\,\sigma_J}\psi_J(\vec{R},\alpha), \tag{A.10}$$

where σ_J are the pure Coulomb phase-shifts and k is related to the total energy $E = \hbar^2k^2/2\mu$. The partial wave-functions are given by

$$\psi_J(\vec{R},\alpha) = \mathrm{i}^J F_{0J}(R)\,Y_{J0}(\theta,\phi)\,\Phi_{00}(\alpha) + \sum_\ell \sum_m C^{J\,2\,\ell}_{0\,-m\,m}\mathrm{i}^\ell F^{(J)}_{2\ell}(R)\,Y_{\ell m}(\theta,\phi)\,\Phi_{2m}(\alpha). \tag{A.11}$$

In (A.11), Φ_{00} and Φ_{2m}, which are related to F_{0J} and $F^{(J)}_{2\ell}$, respectively, are the intrinsic wave-functions for the ground-state and first 2^+ excited state of the ^{12}C. The sum over the Clebsh–Gordan coefficients, $C^{J\,2\,\ell}_{0\,-m\,m}$, warrants the angular momentum conservation.

Taking into account the properties of the intrinsic wave-functions, it is possible to demonstrate (see e.g. [25]) that the non vanishing terms in (A.11) correspond only to $\ell = J-2$, J and $J+2$ (with, of course, $\ell \geqslant 0$). Replacing Ψ in (A.9) by (A.10) and (A.11), the set of coupled equations (1) and (2) of section 3 is obtained. In (2), β_N and β_C actually represent the root–mean–square (rms) values of the nuclear and Coulomb deformations [25, 26]. In our calculations, we have assumed the β_C parameter from its relation with the $B(E2)\uparrow$

$$B(E2)\uparrow = \left(\frac{3Ze\beta_C R_0^2}{4\pi}\right)^2. \tag{A.12}$$

Considering $B(E2)\uparrow = 0.0041\,e^2\mathrm{b}^2$ for ^{12}C [31], we obtain $\beta_C = 0.76$. The β_N parameter was considered an adjustable value in order to fit the data.

Due to the long range of the Coulomb potential, the wave-functions must have the asymptotic behavior expressed by (3) and (4). The reaction and total inelastic cross sections can be obtained from

$$\sigma_\mathrm{R} = \frac{\pi}{k^2}\sum_J (2J+1)(1-|S_{0J}|^2), \tag{A.13}$$

$$\sigma_\mathrm{In} = \frac{\pi k'}{k^3}\sum_J (2J+1)\sum_\ell |S_{2\ell}|^2, \tag{A.14}$$

where $E - E^* = \hbar^2k'^2/2\mu$. Considering the definition (13) of the equivalent PP, the reaction cross section can also be obtained from $\sigma_\mathrm{R} = \sum \sigma_{RJ}$, where [22]:

$$\sigma_{RJ} = -(2J+1)\frac{4\pi}{kE}\int_0^\infty [W(R) + W_\mathrm{pol}(R)]|F_{0J}|^2\,\mathrm{d}R. \tag{A.15}$$

For vanishing imaginary potential, $W(R) = 0$, there is flux conservation (lost of flux in the elastic channel = gain of flux in the inelastic channel) and $\sigma_\mathrm{R} = \sigma_\mathrm{In}$. For $W(R) \neq 0$, part of the flux is absorbed by the imaginary potential, which we associatewith the capture reaction: $\alpha + {}^{12}\mathrm{C} \rightarrow {}^{16}\mathrm{O} + \gamma$. In principle, this flux could be calculated from $\sigma_\mathrm{C} = \sigma_\mathrm{R} - \sigma_\mathrm{In}$. However, σ_C is very small (therefore $\sigma_\mathrm{R} \approx \sigma_\mathrm{In}$) and the corresponding numerical calculation can become quite imprecise. Thus, we prefer to calculate the capture cross section by the equivalent and alternative (12) of section 3.

References

[1] Satchler G R 1983 *Direct Nuclear Reactions* (Oxford: Clarendon Press)
[2] Satchler G R 1997 *Phys. Rep.* **285** 143
[3] Brandan M E and Satchler G R 1991 *Phys. Rep.* **199** 147
[4] Chamon L C, Carlson B V and Gasques L R 2011 *Phys. Rev.* C **83** 034617
[5] Chamon L C, Gasques L R and Carlson B V 2011 *Phys. Rev.* C **84** 044607
[6] Schürmann D, Gialanella L, Kunz R and Strieder F 2012 *Phys. Lett.* B **711** 35
[7] Mitchel I V and Ophel T R 1965 *Nucl. Phys.* **66** 553
[8] Ophel T R, Martin P, Cloud S D and Morris J M 1971 *Nucl. Phys.* A **173** 609
[9] deBoer R J, Couture A, Detwiler R, Gorres J, Tischhauser P, Uberseder E, Ugalde C, Stech E, Wiescher M and Azuma R E 2012 *Phys. Rev.* C **85** 045804
[10] Ames L L 1982 *Phys. Rev.* C **25** 729
[11] Larson J D and Spear R H 1964 *Nucl. Phys.* **56** 497
[12] Schürmann D *et al* 2005 *Eur. Phys. J.* A **26** 301
[13] Frawley A D, Bray K H and Ophel T R 1978 *Nucl. Phys.* A **294** 161
[14] Schardt A, Fowler W A and Lauritsen C C 1952 *Phys. Rev.* **86** 527
[15] Redder A, Becker H W, Lorenz-Wirzba H, Rolfs C, Schmalbrock P and Tratvetter H P 1982 *Z. Phys.* A **305** 325
[16] Marvin T P and Singh P P 1972 *Nucl. Phys.* A **180** 282
[17] Tischhauser P *et al* 2009 *Phys. Rev.* C **79** 055803
[18] Bruno M D, Massa I, Uguzzoni A, Vannini G, Verondini E and Vitale A 1975 *Nuovo Cimento* **27** 1
[19] Plaga R, Becker H W, Redder A, Rolfs C and Trautvetter H P 1987 *Nucl. Phys.* A **465** 291
[20] Morris J M, Kerr G W and Ophel T R 1968 *Nucl. Phys.* A **112** 97
[21] Abramowitz M and Stegun I A 1964 *Handbook of Mathematical Functions* (New York: Dover)
[22] Satchler G R, Nagarajan M A, Lilley J S and Thompson I J 1987 *Ann. Phys.* **178** 110
[23] Thompson I J, Nagarajan M A, Lilley J S and Smithson M J 1989 *Nucl. Phys.* A **505** 84
[24] deBoer R J, Gorres J, Imbriani G, LeBlanc P J, Uberseder E and Wiescher M 2013 *Phys. Rev.* C **87** 015802
[25] Buck B, Stamp A P and Hodgson P E 1963 *Phil. Mag.* **8** 1805
[26] Chamon L C and Carlson B V 2010 *Nucl. Phys.* A **846** 1
[27] Takigawa N, Rumin T and Ihara N 2000 *Phys. Rev.* C **61** 044607
[28] Chamon L C, Nobre G P A, Pereira D, Rossi E S, Silva C P, Gasques L R and Carlson B V 2004 *Phys. Rev.* C **70** 014604
[29] Carlson B V, Chamon L C and Gasques L R 2004 *Phys. Rev.* C **70** 057602
[30] De Vries H, De Jager C W and De Vries C 1987 *At. Data Nucl. Data Tables* **36** 495
[31] Raman S, Malarkey C H, Milner W T, Nestor C W and Stelson P H 1987 *At. Data Nucl. Data Tables* **36** 1